

# Spatial Coherence in Electron-Beam Patterning

Ginusha M. Perera,<sup>†</sup> Gila E. Stein,<sup>†,\*</sup> J. Alexander Liddle<sup>‡</sup>

<sup>†</sup> Department of Chemical and Biomolecular Engineering, University of Houston, Houston TX 77204

<sup>‡</sup> Center for Nanoscale Science and Technology, National Institute of Standards and Technology,

Gaithersburg MD 20899

\*Corresponding author: [gestein@uh.edu](mailto:gestein@uh.edu)

## Abstract

We demonstrate a simple method to identify noise sources in electron-beam systems and accurately quantify the resulting errors in feature placement. Line gratings with a 46 nm average pitch were patterned with electron-beam lithography (EBL) and measured with transmission x-ray diffraction (XRD) and scanning electron microscopy (SEM). All SEM micrographs were analyzed in Fourier space to facilitate comparison with XRD data. Diffraction profiles and Fourier transforms of SEM micrographs contained numerous “satellite” peaks, meaning weak peaks adjacent to the strong primary nodes, that are characteristic of periodic extensions and compressions in the grating pitch. The wavelength and amplitude of these pitch variations were calculated with a simple scaling law by comparing the positions and intensities of satellite peaks relative to their neighboring primary nodes. This approach is remarkably easy to implement because it does not require any modeling of electron density profiles. Data were used to calculate the frequency of each noise source and the resulting variations in grating pitch. Two persistent noise frequencies were detected in the tool studied,  $(62 \pm 2)$  Hz and  $(86 \pm 3)$  Hz, and the tool manufacturer identified likely noise sources as electromagnetic and mechanical in nature, respectively. The 60 Hz noise produced errors in a 46 nm grating pitch of  $3\sigma = 1.5$  nm, where  $\sigma$  is the standard deviation in the grating pitch. Errors due to the 86 Hz noise ranged from  $3\sigma = 1.5$  nm to 2.5 nm. Variations of these magnitudes can be expected to have adverse effects on coupling efficiencies, cavity quality factors, and center wavelength values in photonic devices.

## 1 Introduction

Electron beam lithography (EBL) is a maskless technology for patterning at the nanoscale that is popular for research, development, and manufacturing of nanostructured devices. EBL patterns a radiation-sensitive film called a “resist” by scanning a tightly-focused electron beam across the surface of the sample. This serial exposure process is illustrated in Figure 1, where the circles denote each “pixel” exposed to the electron beam. The resist solubility is altered by exposure to radiation, so subsequent immersion in a developer selectively removes either the exposed (positive-tone) or unexposed (negative-tone) material. EBL is commonly used for patterning semiconductor devices,<sup>1</sup> plasmonic arrays,<sup>2</sup> photonic crystals,<sup>3</sup> templates for directed assembly,<sup>4</sup> and imprint templates.<sup>5</sup>

Advances in EBL technology have focused on reduction in feature size through system design and resist processing,<sup>6</sup> but there have been few efforts to control feature *placement* over large distances. These trends are partly driven by the needs of the semiconductor industry, where local feature overlay is more critical than long-range spatial coherence. However, precise long-range pattern placement is important for micro- and nano-phonic devices that rely on coherent interference effects, and nanoscale variations in critical dimension (pitch) will likely impact the performance of next-generation devices.<sup>7</sup> Electron-beam lithography systems operate with an open-loop control scheme, which means they cannot reference the beam location during an exposure.<sup>8,9</sup> As such, noise during the exposure will displace the pattern elements from their design positions.

We demonstrate that noise during the EBL exposure introduces *periodic* errors in feature placement that are detected with transmission x-ray diffraction (XRD) and Fourier analysis of scanning electron microscopy (SEM) images. A simple method is described to identify the noise

sources and calculate the standard deviation in grating pitch using either XRD or SEM data. Line gratings were patterned with a 46 nm average pitch using electron-beam lithography. The resist was a 33 nm thick film of poly(methylstyrene-*co*-chloromethyl acrylate), commonly known as “ZEP” manufactured by Zeon Chemicals. A representative SEM micrograph of a 46 nm pitch line grating is shown in Figure 2a. The key EBL patterning conditions are summarized in Table 1, and full sample preparation details are provided in the Experimental Procedures section. The only parameter varied between samples is the exposure dose, which ranges from  $950 \mu\text{C}/\text{cm}^2$  up to  $1310 \mu\text{C}/\text{cm}^2$ . This allows for systematic changes in the speed of the pattern generator (i.e., changes the time required to pattern each line in the grating), which is necessary to identify the noise sources during electron-beam patterning.

The first part of this paper describes XRD experiments, models, and data analysis. XRD is a popular technique for characterizing nanostructured thin films because it offers better accuracy, resolution, and statistics than microscopy. Line gratings were measured using synchrotron soft x-ray radiation with wavelength  $\lambda = 4.59 \text{ nm}$ .<sup>10</sup> The diffraction geometry is illustrated in Figure 2b. Diffraction profiles contain numerous “satellite” peaks, meaning weak diffraction peaks adjacent to the strong primary nodes, that are characteristic of periodic extensions and compressions in the grating pitch. These features are illustrated in Figures 2c-d. The wavelengths and amplitudes of pitch variations were determined with a simple scaling law by measuring the positions and intensities of satellite peaks relative to their adjacent primary nodes. The wavelength of pitch variations depends on the EBL exposure frequency, or the time required to pattern each line in the grating, and can therefore identify noise sources that are present during lithography. XRD samples an area of approximately  $500 \mu\text{m} \times 300 \mu\text{m}$ , or roughly 20 minutes of EBL exposure time, so persistent noise sources are detected with this method.

The second part of this paper describes Fourier analysis of SEM measurements. SEM is a popular metrology technique for resist inspection and is widely available in industry and academia. Images are acquired by scanning an electron beam across the surface of the sample and detecting the secondary electron yield with an in-lens detector. Beam positioning is determined with an open-loop control scheme, so the position of elements within the image can be affected by external noise sources. Fourier transforms of SEM micrographs contain numerous satellite peaks that are similar to the features observed in XRD data. The positions of satellites are slightly distorted by noise during the SEM measurement, but the wavelengths and magnitudes of periodic displacements in grating pitch are determined with a confidence of  $\pm 30\%$ , and the sources of noise during EBL patterning are reliably identified. SEM samples an area of approximately  $4\mu\text{m} \times 4\mu\text{m}$ , or roughly 0.2 seconds of EBL exposure time, so both intermittent and persistent noise could be detected with this method.

## 2 Analysis of X-ray Diffraction Data

Our objective is to characterize periodic extensions and compressions in grating pitch that result from noise during electron-beam patterning. This section describes a simple method to measure the wavelength and amplitude of such displacements with x-ray diffraction. Quantitative analysis of diffraction data usually requires a complex model for the wave amplitudes: For example, the diffracted intensity from a simple line grating is a function of nanostructure shape, size, periodicity, and edge roughness.<sup>11–15</sup> However, the methods described in this paper are easy to implement because they do not require any modeling of the diffracted wave amplitudes: Instead, the calculations are based on comparing the positions and intensities of the primary diffraction peaks with their adjacent “satellites.” The following paragraphs briefly introduce

the relevant theory and assumptions required to interpret the diffraction data. Notation is summarized in Table 2.

The diffracted intensity from a resist line grating with density profile  $\rho(\vec{r})$  is:

$$I(\vec{q}) = I_m(\vec{q}) + I_d(\vec{q}) = |\langle \tilde{\rho}(\vec{q}) \rangle|^2 + \langle |\tilde{\rho}(\vec{q}) - \langle \tilde{\rho}(\vec{q}) \rangle|^2 \rangle \quad (1)$$

Note that  $\tilde{\rho}(\vec{q})$  is the Fourier transform of  $\rho(\vec{r})$ ,  $\vec{r} = \{x, y, z\}$  is the real-space position vector, and  $\vec{q} = \{q_x, q_y, q_z\}$  is the scattering vector.  $I_m(\vec{q})$  is the scattering from the mean density profile, and reflects the average pitch, line width, sidewall angle, and line-edge roughness of the gratings across the sampled area.  $I_d(\vec{q})$  is the diffuse scattering from concentration defects or lattice disorder. In general, diffuse scattering is difficult to distinguish from background noise in the measurement. However, *periodic* displacements in the grating pitch produce weak satellite peaks that are easily identified in the diffraction data.<sup>16</sup> Primary and satellite peaks are illustrated in Figures 2b-2d.

The mean density profile  $\langle \rho(\vec{r}) \rangle$  is modeled by convolving a one-dimensional lattice  $\delta_n(x - nd)$  with a function  $s(\vec{r})$  that describes the average size, shape, and line-edge roughness of the gratings. The mean diffracted intensity is:

$$I_m(\vec{q}) = \sum_{n=-\infty}^{n=\infty} \delta(q_x - 2\pi n/d) \cdot |\tilde{s}(\vec{q})|^2 \cdot |\tilde{h}(\vec{q})|^2 \quad (2)$$

Diffraction from the mean density profile is observed at discrete positions  $q_{x,n} = 2\pi n/d$ , and we refer to these features as the *primary peaks*. The function  $|\tilde{s}(\vec{q})|^2$  is the “form factor,” and describes the shape of the resist cross-section. The function  $|\tilde{h}(\vec{q})|^2$  describes the attenuation of the diffraction signal due to line-edge roughness.

The diffuse scattering from periodic changes in pitch is described by Guinier:<sup>16</sup> Displacements in the grating pitch at a point  $x_n$  are described by the wave  $\Delta\vec{x}_n = \vec{A}\cos(\vec{k}\cdot\vec{x}_n)$ , where  $\vec{A}(= \epsilon/k_x)$  is the amplitude and  $\vec{k}$  is the propagation vector. The grating pitch then varies sinusoidally from  $d(1 - \epsilon)$  to  $d(1 + \epsilon)$ , which is illustrated in Fig 2(b). If the amplitudes of the displacements are small, i.e.,  $\epsilon \ll 1$ , then the scattering from the mean density profile  $I_m$  and the diffuse scattering from the satellites  $I_{sat}$  are:

$$I_m(\vec{q}) = I(\vec{q}) \{1 - q_x^2 \epsilon^2 k_x^{-2} / 4\} \quad (3)$$

$$I_{sat}(\vec{q}) = I(\vec{q} \pm \vec{k}) \{q_x^2 \epsilon^2 k_x^{-2} / 4\} \quad (4)$$

The satellite peaks in the resist data are positioned adjacent to primary nodes at  $q_{x,n} \pm k_x$ . The propagation vector modulus ( $|\vec{k}| = k_x = 2\pi/\Lambda$ ) is therefore calculated from the positions of satellite peaks relative to their adjacent primary nodes. These features are illustrated in Figure 2b-d.

The parameter  $\epsilon$  is calculated from Equations 3-4 using two approximations: First, if the form factor does not sharply vary near the primary peaks, we can write  $|\tilde{s}(\vec{q})|^2 \simeq |\tilde{s}(\vec{q} \pm \vec{k})|^2$ . This approximation is valid if the positions of primary peaks do not coincide with minima in the form factor. Second, we note that line-edge roughness slowly damps the intensity with increasing  $q_x$ , so the approximation  $|\tilde{h}(\vec{q})|^2 \simeq |\tilde{h}(\vec{q} \pm \vec{k})|^2$  is always valid. These simplifications lead to the following result:

$$I_{sat}/I_m \simeq q_x^2 \epsilon^2 / 4k_x^2 \quad (5)$$

The scaling law described by Equation (5) provides a simple method to calculate  $\epsilon$  from the relative intensity of satellite to primary peaks, eliminating the need for complex models to

describe resist sidewall angle, line-edge roughness, and size polydispersity. The XRD Results section includes a comparison between the simple scaling law and diffraction models that include the wave amplitudes according to Equations (3)-(4). The results are identical within experimental error.

### 3 Fourier analysis of SEM images

The objective of SEM image analysis is to characterize the periodic extensions and compressions in grating pitch that result from noise during electron-beam patterning. Quantitative interpretation of SEM micrographs is difficult due to the complex image formation process:<sup>17</sup> For example, the edges of resist lines appear “brighter” due to increased secondary electron yield and can lead to erroneous calculations of line width.<sup>15</sup> It is therefore difficult to calculate the size, shape, and edge-roughness of a resist line based on a SEM measurement. However, it is straightforward to detect periodic structures in an image using Fourier analysis. The Fourier transform of an SEM micrograph can be modeled with Equation 2, although the function  $|\tilde{s}(\vec{q})|^2$  reflects the spatial distribution of secondary electron yield rather than the resist form factor. Satellite peak locations are set by the wavelengths of extensions and compression in grating pitch, and satellite peak amplitudes are largely determined by the magnitude of displacements in the grating pitch. The approximations used to derive Equation (5) are valid for Fourier analysis of SEM images, but difficulties arise when distortions in the SEM image shift the positions and intensities of the satellite peaks relative to the primary nodes. Distortions may result from noise during SEM measurements, resist charging, or undersampling.

## 4 Noise Frequencies during EBL

Our objective is to identify the noise sources that produce pattern placement errors in the electron beam lithography exposure. The noise frequency  $\omega_i$  is calculated from the number of lines per noise cycle ( $\Lambda/d$ ) and the time required to expose each line (the speed of the pattern generator). The wavelength  $\Lambda$  is measured from the data, while the following parameters are specified by the exposure conditions: Grating pitch  $d$ , dose, beam current  $c$ , pixel size  $p$ , line length  $L$ , and the number of passes per line  $N_p$ .

$$\omega_i = \frac{\text{cycles}}{\text{time}} = \left( \frac{\text{lines}}{\text{cycle}} \frac{\text{steps}}{\text{line}} \frac{\text{time}}{\text{step}} \right)^{-1} = \left( \frac{\Lambda}{d} \frac{N_p \times L}{p} \frac{\text{dose} \times p^2}{c} \right)^{-1} \quad (6)$$

The Results and Discussion sections includes XRD and SEM measurements from nanoscale line gratings exposed at different doses while all other conditions were held constant. We expect to see  $\Lambda/d$  scale with dose as follows:

$$\frac{\Lambda}{d} = \frac{1}{\omega_i} \times \frac{c}{N_p \times L \times p} \times \frac{1}{\text{dose}} \quad (7)$$

## 5 XRD Results

Line gratings with a  $d = 46$  nm pitch were patterned at four exposure doses: 950, 1010, 1070, and 1130  $\mu\text{C}/\text{cm}^2$ . All other exposure parameters were the same for each sample and are summarized in Table 1. Representative XRD data from line gratings are shown in Figures 3a-3b. Two distinct satellite peaks were always observed in the diffraction data, which indicates that two persistent noise sources were present during the electron-beam patterning. These two satellites are visible in Figure 3c.

Three methods of analysis were used to determine primary peak positions  $q_{x,n}$ , satellite

positions  $q_{x,n} \pm k_{x,i}$ , primary amplitudes  $I_m(q_{x,n})$ , and satellite amplitudes  $I_{\text{sat}}(q_{x,n} \pm k_{x,i})$  from each data set. The parameters  $k_{x,i}$  are the frequencies of periodic extensions and compressions in the pitch and are needed to calculate noise sources  $\omega_i$  using Equation 7. The parameters  $q_{x,n}$ ,  $k_{x,i}$ ,  $I_m(q_{x,n})$ , and  $I_{\text{sat}}(q_{x,n} \pm k_{x,i})$  are all needed to calculate  $\epsilon$  by Equation 5. Note that the standard deviation in the grating pitch is  $\sigma \simeq d\epsilon$ . The three methods for diffraction data analysis are as follows:

1. Satellite peak positions and intensities were obtained by visual inspection of the diffraction data. A “point-and-click” algorithm was implemented in Matlab where the user identified each peak by visual inspection and the software recorded the position and intensity of each peak. The parameter  $\epsilon$  is then calculated for each set of diffraction data using Equation (5).
2. Peak positions and intensities were fit with an automated routine based on the  $q^2$ -scaling law of Equation (5). The “point-and-click” algorithm is used to acquire initial guesses for peak positions and amplitudes. The software fits a Gaussian function to each primary peak to calculate the position  $q_x$  and intensity  $I_m(q_x)$ . The software automatically detects the positions of adjacent satellites  $q_x \pm k_x$  and fits the satellites to a Gaussian function, where the Gaussian peak amplitude  $I_{\text{sat}}(q_x \pm k_x)$  is constrained according to the scaling law of Equation 5, and regression analysis uses  $\epsilon$  as an adjustable parameter. Representative experimental data are shown in Figures 3a-3c with fits to the  $q^2$ -scaling law.
3. For comparison, diffraction data were fit using the models described by Equations 2-4. This approach calculates the peak intensities as a function of the size, shape, and line-edge roughness of the resist patterns. Full details are provided elsewhere.<sup>15</sup>

The first objective is to calculate the wavelengths ( $\Lambda_i = 2\pi/k_{x,i}$ ) of periodic displacements

in grating pitch as a function of exposure dose. Results are summarized for each satellite peak in Figure 4. Red, blue, and green data points were acquired with analysis methods 1, 2, and 3, respectively. The wavelengths are on the order of  $10d$  and decrease linearly with increasing exposure dose, which is the scaling expected based on Equation (7).

The second objective is to identify the noise frequencies  $\omega_i$  that are present during EBL from the dependence of  $\Lambda_i/d$  on exposure dose. The data shown in Figure 4a were fit to Equation (7) using the noise frequency  $\omega_i$  an adjustable parameter. The two noise frequencies determined with Equation (7) are  $\omega_1 = (62 \pm 2)$  Hz and  $\omega_2 = (86 \pm 3)$  Hz, and results from each method of analysis agree within the reported error.

The third objective is to calculate the standard deviation in grating pitch ( $\sigma \simeq d\epsilon$ ), which requires that we validate the  $q^2$ -scaling proposed in Equation (5) in order to calculate  $\epsilon$ . Peak positions and intensities were detected with the “point-and-click” algorithm, and then plots were generated to establish the scaling of  $\log(I_{\text{sat}}k_x^2/I_m)$  vs.  $\log(q_x)$ . Examples of these data are shown in Figures 5a-5b for a grating exposed at  $950 \mu\text{C}/\text{cm}^2$ . The gradient of these plots is equal to  $2.0 \pm 0.1$ , which is the value predicted by the  $q^2$ -scaling law, and the value of  $\epsilon$  is determined from the y-intercept. Diffraction profiles were also fit with the automated algorithm described in Method 2, which enforces the  $q^2$ -scaling law, and representative results are included in Figure 3a-3b. Diffraction profiles fit by Method 3 to Equations (3)-(4) are published elsewhere.<sup>15</sup> The semiconductor industry quotes line width and overlay tolerances in terms of  $3\sigma$ , so results for  $3\sigma$  as a function of exposure dose are summarized in Figure 6a. Red, blue, and green data points were acquired with analysis methods 1, 2, and 3, respectively. All methods of analysis closely agree, and  $3\sigma$  values for each noise frequency range from 1.5 nm to 2.5 nm.

## 6 SEM Results

Line gratings with a  $d = 46$  nm pitch were patterned using exposure doses in the range of 950-1310  $\mu\text{C}/\text{cm}^2$  and imaged with SEM as described in the Experimental Procedures section. The two-dimensional discrete Fourier transform was calculated for each image, where the output is the squared magnitude, and representative results are shown in Figures 3d-3e. SEM data typically contain more satellite peaks than XRD profiles, which is apparent in Figure 3f, but our analysis is focused on the two satellite peaks that are observed in all data sets.

The first objective is to calculate the wavelengths of periodic displacements in grating pitch from each image. The positions of satellite peaks in the SEM data were slightly distorted, meaning the values of  $k_{x,i}$  varied by 30 % within a single image, so all calculations used the average  $k_{x,i}$  values determined by the “point-and-click” algorithm. Results for  $\Lambda_i/d$  as a function of exposure dose are summarized in Figure 4b. Wavelengths determined from SEM analysis match the XRD results.

The second objective is to identify the noise frequencies  $\omega_i$  responsible for errors in EBL patterns. Data for  $\Lambda_i/d$  as a function of exposure dose were fit to Equation (7) using the noise frequency  $\omega_i$  as an adjustable parameter. The two frequencies calculated from SEM data are  $\omega_1 = (65 \pm 1)$  Hz and  $\omega_2 = (87 \pm 1)$  Hz, respectively, which are consistent with XRD results.

The third objective is to calculate the standard deviation in grating pitch ( $\sigma \simeq d\epsilon$ ) from analysis of the SEM Fourier transforms. The peak positions and amplitudes were recorded with the “point-and-click” algorithm, then plots were generated to determine the scaling of  $\log(I_{\text{sat}}k_x^2/I_m)$  vs.  $\log(q_x)$ . Figure 5c includes examples from two data sets along with best-fit lines. Neither data set follows the  $q^2$ -scaling predicted by Equation (5), so the parameter  $\epsilon$  cannot be calculated from the y-intercept value. Figures 3d-3e shows examples of SEM data

with “forced” fits to the  $q^2$ -scaling law using  $\epsilon$  as an adjustable parameter. This procedure is the same as Method 2 for analysis of XRD profiles, except that satellite peak positions  $k_{x,i}$  are constrained to their average measured value from the “point-and-click” algorithm. The values of  $\epsilon$  calculated with this approach are remarkably consistent with XRD analysis, even though SEM data exhibit poor agreement with the model. Results for  $3\sigma$  as a function of exposure dose are summarized in Figure 6b.

## 7 Discussion

The wavelengths calculated from XRD and SEM measurements agree within experimental error and range from  $5d - 10d$ . These wavelengths are specific to the tool studied and the exposure conditions summarized in Table 1. The wavelengths calculated for each exposure dose were used to identify the noise sources responsible for EBL errors, and two frequencies were detected in all data sets at approximately 62 Hz and 86 Hz. All laboratory equipment runs on 60 Hz mains power, so the source of 62 Hz noise is likely electromagnetic. A vibrating component within the electron-beam exposure tool was identified as the source of the  $\sim 86$  Hz noise.<sup>18</sup> Additional noise frequencies at 55 Hz and 150 Hz were detected in most SEM data and about half of the XRD data, but their sources could not be identified.

In general, the Fourier transforms of SEM data contained more satellite peaks than XRD profiles, even though many of the SEM images that we analyzed were acquired from the same samples measured by XRD. SEM measurements capture a small area of the gratings relative to XRD ( $\sim 0.01\%$ ), reflecting a small window of time from the EBL exposure. The appearance of additional satellites in SEM data may indicate an intermittent noise source. It is also possible that noise during SEM imaging produces apparent displacements in the grating. Noise in the

SEM instrument could be detected by imaging the same area with different scan rates and analyzing results with a modified form of Equation (6).

The standard deviations in grating pitch are calculated from the  $q^2$ -scaling law described by Equation (5). This procedure simplifies data analysis by eliminating any need to model resist density profiles for XRD or secondary electron yield for SEM. The data shown in Figures 5a-5b demonstrate that XRD profiles are consistent with the scaling law. The minimal scatter of data points about the best-fit line is due to changes in the resist form factor near the primary peaks. Figure 6a summarizes the standard deviation calculated from XRD profiles using three methods of data analysis: Visual inspection based on the “point-and-click” algorithm, the automated routine based on Equation (5), and modeling the resist form factor and line-edge roughness with Equations (3)-(4). All three methods agree, and this comparison demonstrates that the  $q^2$ -scaling without form factor corrections is appropriate for XRD analysis. In general, the SEM data are poorly modeled by Equation (5). This may be partly attributed to errors in satellite peak positions that are “amplified” through the dependence of Equation (5) on  $k_x^2$ . It is interesting to note that fitting the Fourier transforms of SEM images with the  $q^2$ -scaling law produces values of  $\epsilon$  that match the outcome of XRD analysis, despite the poor agreement between model and data. The variations in grating pitch reported in Figures 6a-6b range from 1.5 nm up to 2.5 nm ( $3\sigma$ ). The magnitude of these errors are significant in the context of semiconductor manufacturing requirements: More than 4 different “critical” exposures are required to pattern an integrated circuit, and if each step introduce a small error then it will be difficult to achieve overlay with nanometer precision. The periodic changes in pitch are also significant for photonic devices, where nanoscale variations can impact the coupling efficiencies, cavity quality factors, and center wavelength values.<sup>2,3,19</sup>

The noise frequencies that can be identified with XRD and SEM are determined by both

the resolution of the experiment and the design parameters of the grating. The minimum and maximum values of  $k_x$  that can be detected were determined as follows: The minimum  $k_x$  value is the closest satellite peak position that can be distinguished from the primary peak. The maximum  $k_x$  value is the satellite peak position that is farthest from the associated primary peak but can be distinguished from neighboring primary peaks (i.e.,  $k_x < 2\pi/d$ ). The minimum/maximum noise frequencies that can be detected with our experiments were calculated using Equation 7 and range from approximately 20 Hz up to 500 Hz, and are summarized in Table 3 as a function of exposure dose. It is straightforward to change the patterning conditions to probe different frequency limits using Equation (7) as a guide.

## 8 Conclusions

Periodic noise during an electron beam lithography exposure can displace the pattern elements from a perfect grid. We present a simple method to measure the structure of these displacements and identify the noise sources responsible for errors in pattern placement. Line gratings with a 46 nm pitch were patterned with EBL and measured with x-ray diffraction (XRD) and scanning electron microscopy (SEM). XRD profiles and Fourier transforms of SEM micrographs contained satellite peaks, meaning weak peaks adjacent to the primary nodes, that signify periodic changes in the lattice pitch. Wavelengths and amplitudes of these periodic displacements were calculated with a simple scaling law that only required peak positions and intensities as input. Two persistent noise frequencies were identified,  $(62 \pm 2)$  Hz and  $(86 \pm 3)$  Hz, and frequencies near 55 Hz and 150 Hz were also detected in a few data sets. The experiments can detect noise in the range of 25 Hz to 500 Hz, and the exposure parameters (grating pitch, exposure frequency, etc.) could be changed to probe different limits. The EBL

instrument noise produced errors in a 46 nm grating pitch of  $3\sigma = 1$  nm to 3 nm, where  $\sigma$  is the standard deviation in the grating pitch. These errors are significant for photonic and plasmonic devices that rely on coherent interference for operation.

**Acknowledgements.** We appreciate financial support from the NSF ENG EEC/ECCS Program under Award No. 0927147 and the UH GEAR Program under Award No. 98520. The Advanced Light Source is supported by the Director, Office of Science, Office of Basic Energy Sciences, of the U.S. Department of Energy under Contract No. DE-AC02-05CH11231. Research was performed in part at the NIST Center for Nanoscale Science and Technology. We thank W. L. Wu and C. Q. Wang for helpful discussions.

## 9 Experimental Procedures

Certain materials and procedures are identified in this paper in order to specify the experimental procedure adequately. Such identification is not intended to imply recommendation or endorsement by the authors or their institutions, nor is it intended to imply that the materials or procedures identified are the best available for the purpose.

**Substrate Fabrication** XRD experiments require a transparent substrate, so we fabricate all samples on silicon nitride (SiN) membranes that are approximately 50 % transparent to 270 eV radiation. A 100 nm thick film of low-stress (silicon rich) SiN is deposited on clean  $\langle 100 \rangle$  silicon wafers using low-pressure chemical vapor deposition with the following parameters:  $7.44 \times 10^{-5}$  mol/sec (100 sccm) dichlorosilane,  $1.49 \times 10^{-5}$  moles/s (20 sccm) ammonia, 33 Pa (250 mT), and 835 °C. The deposition rate is 6.9 nm/min, and the film stress is  $(170 \pm 10)$  MPa tensile. The front side of the substrates is then patterned with gold “alignment marks”

that are aligned with the crystallographic axes of the silicon wafer. These marks are used to define the position and orientation of the electron beam lithography patterns, which ensures the patterned gratings are properly aligned with the x-ray beam. The backside of each wafer is patterned with an array of “windows” where the SiN film is removed with a CHF<sub>3</sub> reactive ion etch. Membranes are created by etching away the silicon in the “window” areas with a 0.3 g/g mass fraction potassium hydroxide solution (aqueous) at 40 °C for 2 days. The resulting membranes span 1 mm ×1 mm. The backside of the membranes is then coated with 400 nm of aluminum, which is necessary to ensure a uniform substrate thermal conductivity for spin-casting and bake processes. (Note that aluminum is removed prior to XRD measurements).

**Electron beam lithography** Substrates were spin coated with a 33 nm thick film of poly(methyl styrene-*co*-chloromethyl acrylate) electron beam resist (ZEP, Zeon Chemicals) and baked at 180 °C for 2 minutes. Line gratings were patterned using an accelerating voltage of 100 keV, beam current of 1.1 nA, and beam step size of 2 nm. The design line width was 12 nm (6-passes), and the design pitch was 46 nm. Exposure dose was varied from 950 to 1130  $\mu\text{C}/\text{cm}^2$  for preparation of XRD samples. A broader dose range of 950  $\mu\text{C}/\text{cm}^2$  to 1310  $\mu\text{C}/\text{cm}^2$  was used for SEM analysis. The coherence length of the gratings is determined by the length of the beam deflection, which was set to 16  $\mu\text{m}$ . An area of 1 mm ×1 mm was patterned by stitching together 62 gratings that spanned 16  $\mu\text{m}$  ×16  $\mu\text{m}$ . The ZEP resist was developed in hexyl acetate at -6 °C for 40 seconds, followed by a 10 second rinse in isopropyl alcohol and dried in nitrogen. After pattern development, aluminum coatings are rinsed off the back of membranes using 0.45 g/g mass fraction potassium hydroxide solution (aqueous) at room temperature.

**X-ray Diffraction** Transmission x-ray diffraction (XRD) measurements were completed at the Advanced Light Source beam line 6.3.2 using a photon energy of 270 eV ( $\lambda = 4.59$  nm). The scattering geometry is illustrated in 2. The sample is illuminated at normal incidence, and the scattering is recorded by scanning a channel electron multiplier detector mounted on a rotating arm from  $2^\circ - 45^\circ$  in  $0.1^\circ$  increments. The signal is averaged for 10 seconds per angle. Each diffraction measurement samples an area of  $500 \mu\text{m} \times 300 \mu\text{m}$ , and data were recorded from two locations per sample. The lateral coherence length of the radiation is on the order of a few micrometers. The resist grating axis was aligned to the y-axis with an accuracy of  $\pm 1^\circ$ . The elastic scattering vector is  $\vec{q} = \vec{g}_f - \vec{g}_i$ , where  $\vec{g}_f$  and  $\vec{g}_i$  are the incident and scattered wave vectors, respectively. Correcting for refraction at the polymer interfaces, the wave vectors inside the film are defined as  $\vec{g}_i = 2\pi \{ \sin \alpha_i, 0, (n_p^2 - \sin^2 \alpha_i)^{0.5} \} / \lambda$  and  $\vec{g}_f = 2\pi \{ \sin 2\theta, 0, (n_p^2 - \sin^2 2\theta)^{0.5} \} / \lambda$ , where  $n_p$  is the refractive index of the polymer film. The diffracted intensity from a line grating with a rectangular cross-section decays as  $q_x^{-2}$ , so all diffraction data are plotted with the scaling  $Iq_x^2$  vs.  $q_x$  so that higher-order peaks are easier to detect by eye.

**Scanning Electron Microscopy** Scanning electron microscopy (SEM) measurements were completed with an accelerating voltage of 1.5 keV, 2 mm working distance, 30 kx magnification, and scanning speed of 5.1 seconds per frame (approximately 150 Hz). All gratings were oriented with the line axis perpendicular to the scan axis. Data were recored with an in-lens secondary electron detector and stored in  $1024 \times 768$  pixel arrays using grayscale TIFF format. Each image contains approximately 80 resist lines or roughly 10 “noise cycles.” Fourier transforms were calculated for each SEM image, and the squared Fourier magnitudes were used for comparison with XRD data. Note that many of the SEM images were acquired from the

same samples used for XRD measurements.

## References

- [1] R. F. Pease and S. Y. Chou. Lithography and other patterning techniques for future electronics. *PROCEEDINGS OF THE IEEE*, 96(2):248–270, FEB 2008.
- [2] E. M. Hicks, S. L. Zou, G. C. Schatz, K. G. Spears, R. P. Van Duyne, L. Gunnarsson, T. Rindzevicius, B. Kasemo, and M. Kall. Controlling plasmon line shapes through diffractive coupling in linear arrays of cylindrical nanoparticles fabricated by electron beam lithography. *NANO LETTERS*, 5(6):1065–1070, JUN 2005.
- [3] S. Noda, M. Fujita, and T. Asano. Spontaneous-emission control by photonic crystals and nanocavities. *NATURE PHOTONICS*, 1(8):449–458, AUG 2007.
- [4] J. Y. Cheng, C. A. Ross, H. I. Smith, and E. L. Thomas. Templated self-assembly of block copolymers: Top-down helps bottom-up. *ADVANCED MATERIALS*, 18(19):2505–2521, OCT 4 2006.
- [5] H. Schiff. Nanoimprint lithography: An old story in modern times? A review. *JOURNAL OF VACUUM SCIENCE & TECHNOLOGY B*, 26(2):458–480, MAR-APR 2008.
- [6] C. Vieu, F. Carcenac, A. Pepin, Y. Chen, M. Mejias, A. Lebib, L. Manin-Ferlazzo, L. Couraud, and H. Launois. Electron beam lithography: resolution limits and applications. *APPLIED SURFACE SCIENCE*, 164:111–117, SEP 1 2000.
- [7] International technology roadmap for semiconductors. Technical report, 2009. (See sections titled Lithography and Emerging Research Materials).
- [8] B. E. Maile, W. Henschel, H. Kurz, B. Rienks, R. Polman, and P. Kaars. Sub-10 nm linewidth and overlay performance achieved with a fine-tuned EBPB-5000 TFE electron beam lithography system. *JAPANESE JOURNAL OF APPLIED PHYSICS PART 1-*

*REGULAR PAPERS SHORT NOTES & REVIEW PAPERS*, 39(12B):6836–6842, DEC 2000.

- [9] J. T. Hastings, F. Zhang, M. A. Finlayson, J. G. Goodberlet, and H. I. Smith. Two-dimensional spatial-phase-locked electron-beam lithography via sparse sampling. *JOURNAL OF VACUUM SCIENCE & TECHNOLOGY B*, 18(6):3268–3271, NOV-DEC 2000.
- [10] Note that hard x-ray radiation is also suitable for these experiments, and diffraction from line gratings can be measured with a laboratory x-ray source.
- [11] R. L. Jones, T. Hu, E. K. Lin, W. L. Wu, R. Kolb, D. M. Casa, P. J. Bolton, and G. G. Barclay. Small angle x-ray scattering for sub-100 nm pattern characterization. *APPLIED PHYSICS LETTERS*, 83(19):4059–4061, 2003.
- [12] T. J. Hu, R. L. Jones, W. L. Wu, E. K. Lin, Q. H. Lin, D. Keane, S. Weigand, and J. Quintana. Small angle x-ray scattering metrology for sidewall angle and cross section of nanometer scale line gratings. *JOURNAL OF APPLIED PHYSICS*, 96(4):1983–1987, 2004.
- [13] C. Wang, R. L. Jones, E. K. Lin, W.-L. Wu, and J. Leu. Small angle x-ray scattering measurements of lithographic patterns with sidewall roughness from vertical standing waves. *APPLIED PHYSICS LETTERS*, 90(19), MAY 7 2007.
- [14] C. Wang, W.-E. Fu, B. Li, H. Huang, C. Soles, E. K. Lin, W.-L. Wu, P. S. Ho, and M. W. Cresswell. Small angle X-ray scattering measurements of spatial dependent linewidth in dense nanoline gratings. *THIN SOLID FILMS*, 517(20):5844–5847, AUG 31 2009.
- [15] G. E. Stein, J. A. Liddle, A. L. Aquila, and E. M. Gullikson. Measuring the Structure of Epitaxially Assembled Block Copolymer Domains with Soft X-ray Diffraction. *MACRO-MOLECULES*, 43(1):433–441, JAN 12 2010.

- [16] A. Guinier. *X-ray diffraction in crystals, imperfect crystals, and amorphous bodies*. Dover Publications, Inc., 1994. It is possible that the pitch does not vary sinusoidally from  $d(1-\epsilon)$  to  $d(1+\epsilon)$ , but rather exhibits two discrete values  $d(1\pm\epsilon)$ . The latter case would present with higher-order satellite peaks, but they may be too weak to observe.
- [17] J. S. Villarrubia, A. E. Vladar, and M. T. Postek. Scanning electron microscope dimensional metrology using a model-based library. *SURFACE AND INTERFACE ANALYSIS*, 37(11):951–958, NOV 2005.
- [18] Private communication with the instrument manufacturer. the sample holder was identified as the vibrating component.
- [19] C. L. Haynes, A. D. McFarland, L. L. Zhao, R. P. Van Duyne, G. C. Schatz, L. Gunnarsson, J. Prikulis, B. Kasemo, and M. Kall. Nanoparticle optics: The importance of radiative dipole coupling in two-dimensional nanoparticle arrays. *JOURNAL OF PHYSICAL CHEMISTRY B*, 107(30):7337–7342, JUL 31 2003.

## List of Tables

1	Summary of e-beam parameters used to pattern the line gratings. Gratings for XRD span a total area of $1 \text{ mm} \times 1 \text{ mm}$ (62 smaller gratings spanning $16 \text{ }\mu\text{m} \times 16 \text{ }\mu\text{m}$ are stitched together). Gratings for SEM spanned $100 \text{ }\mu\text{m} \times 100 \text{ }\mu\text{m}$ .	26
2	Notation for models described by Equations (1)-(7).	27
3	Minimum ( $\omega_{min}$ ) and maximum ( $\omega_{max}$ ) noise frequencies that are detectable at each exposure dose. Note that these limits are calculated for the specific experimental conditions outlined in the paper, and other frequency ranges are accessible by adjusting the exposure parameters.	28

## List of Figures

1	Schematic illustrating scanning electron-beam lithography. Each circle marks a pixel addressed by the beam, and each line of length $L$ is generated with 6 passes.	29
2	(Full page) (a) Representative SEM measurement of 46 nm pitch line grating with Fourier transform (inset). Resist is ZEP and exposure dose is $950 \text{ }\mu\text{C}/\text{cm}^2$ ; other relevant exposure parameters are summarized in Table 1. (b) Transmission x-ray diffraction geometry. (c) Periodic compressions and extensions of the grating pitch characterized by period $\Lambda = 2\pi/k_x$ . Average pitch is $d$ and the standard deviation is $\sigma \approx d\epsilon$ . (d) Primary diffraction peaks are distributed with periodicity $q_x = 2\pi n/d$ , where $n$ is an integer, and satellite peaks are adjacent to each primary peak at $\pm k_x = 2\pi/\Lambda$ .	30

3	<p>(Full Page) Comparison of XRD data and SEM Fourier transforms. (a,b) Diffraction data from two different ZEP resist gratings and fits to the scaling law in Equation (5). (c) Enlarged region of (b) that shows primary diffraction peaks along with two satellites at <math>k_{x,1} = 2\pi/\Lambda_1</math> and <math>k_{x,2} = 2\pi/\Lambda_2</math>. Satellites marked “1” and “2” are associated with noise frequencies <math>(62 \pm 2)</math> Hz and <math>(86 \pm 3)</math> Hz, respectively. A third satellite peak associated with ca. 150 Hz noise is visible in these data but was not detected in every sample. (d,e) Fourier transforms of SEM data from two different ZEP resist gratings and fits to the scaling law in Equation (5). (f) Enlarged region of (e) shows primary diffraction peaks along with the two satellites. SEM data are significantly noisier than XRD and do not agree with the <math>q^2</math>-scaling law. . . . .</p>	31
4	<p>Noise cycles <math>\Lambda/d</math> for each satellite peak as a function of EBL exposure dose. Solid lines are fits to Equation 7. (a) XRD results. The noise frequencies calculated from visual inspection (red), scaling law (green), and the scaling law with form factor corrections (blue) all closely agree. Error bars represent the uncertainty in determining <math>k_x = 2\pi/\Lambda</math> from the diffraction data, which is <math>0.001 \text{ nm}^{-1}</math> by any method. (b) SEM results. Noise frequencies are calculated from visual inspection; other algorithms fail due to SEM image artifacts. Each data point represents the average value of <math>k_x</math> measured from each image and error bars encompass <math>\pm 1</math> standard deviation. . . . .</p>	32

5	<p>Analysis of ca. 62 Hz and 86 Hz noise in a grating exposed at 950 <math>\mu\text{C}/\text{cm}^2</math>. (a,b) XRD data were analyzed with the “point-and-click” algorithm based on visual inspection. Line is the best fit, and the best-fit slope for both data sets is <math>2.0 \pm 0.1</math>. This is the slope predicted by the scaling law established with Equation (5). (c) SEM data were analyzed with the algorithm based on visual inspection, but results do not follow the scaling predicted by Equation (5). . . .</p>	33
6	<p>The <math>3\sigma</math> variation in grating pitch as a function of EBL exposure dose, where <math>\sigma</math> is the standard deviation. Open and closed symbols correspond with ca. 62 Hz and 86 Hz noise, respectively. (a,b) XRD data analysis. Calculations based on visual inspection (red), scaling law (green), and the scaling law with form factor corrections (blue) all closely agree. Note that 86 Hz noise (mechanical) exhibits greater variation between samples than the 62 Hz noise (electromagnetic). (c) SEM data analysis with the scaling law. Calculated standard deviations are consistent with XRD analysis despite poor agreement between SEM data and the scaling law. . . . .</p>	34

<b>Parameter</b>	<b>Value</b>
Grating pitch ( $d$ )	46 nm
Beam current ( $c$ )	1.1 nA
Area exposure dose (dose)	950-1310 $\mu\text{C}/\text{cm}^2$
EBL pixel size ( $p$ )	2 nm
Passes per line ( $N_p$ )	6
Line length ( $L$ )	16 $\mu\text{m}$

Table 1: Summary of e-beam parameters used to pattern the line gratings. Gratings for XRD span a total area of  $1\text{ mm} \times 1\text{ mm}$  (62 smaller gratings spanning  $16\ \mu\text{m} \times 16\ \mu\text{m}$  are stitched together). Gratings for SEM spanned  $100\ \mu\text{m} \times 100\ \mu\text{m}$ .

$\vec{q}$	Scattering vector, $\text{nm}^{-1}$
$d$	Grating pitch, nm
$\Lambda$	Noise wavelength, nm
$\vec{k}$	Noise propagation vector, $\text{nm}^{-1}$
$\epsilon$	Fractional variation in grating pitch
$\omega$	Noise frequency, Hz
$c$	Beam current, $\mu\text{A}$
dose	Area exposure dose, $\mu\text{C}/\text{cm}^2$
$p$	EBL pixel size, cm
$N_p$	Number of passes per line
$L$	Line length, cm

Table 2: Notation for models described by Equations (1)-(7).

Dose ( $\mu\text{C}/\text{cm}^2$ )	$\omega_{min}$ XRD/SEM (Hz)	$\omega_{max}$ XRD/SEM (Hz)
950	26/17	554/562
1010	26/16	517/526
1070	24/15	488/496
1130	23/14	465/473

Table 3: Minimum ( $\omega_{min}$ ) and maximum ( $\omega_{max}$ ) noise frequencies that are detectable at each exposure dose. Note that these limits are calculated for the specific experimental conditions outlined in the paper, and other frequency ranges are accessible by adjusting the exposure parameters.

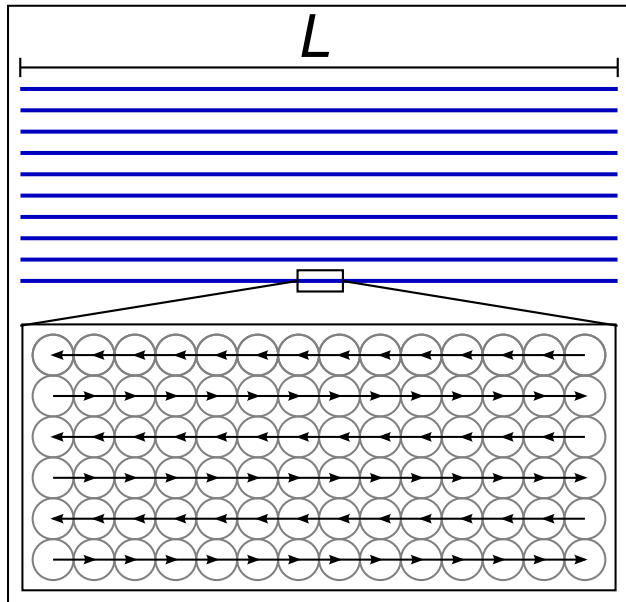


Figure 1: Schematic illustrating scanning electron-beam lithography. Each circle marks a pixel addressed by the beam, and each line of length  $L$  is generated with 6 passes.

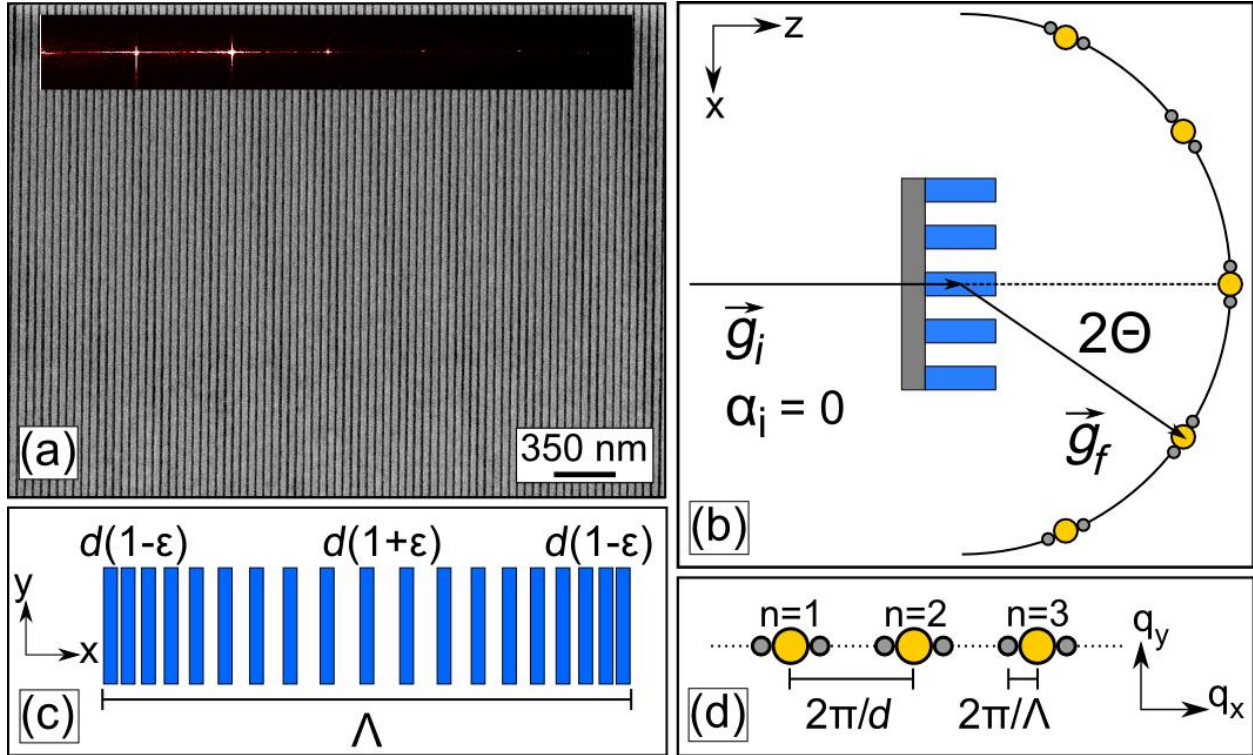


Figure 2: (Full page) (a) Representative SEM measurement of 46 nm pitch line grating with Fourier transform (inset). Resist is ZEP and exposure dose is  $950 \mu\text{C}/\text{cm}^2$ ; other relevant exposure parameters are summarized in Table 1. (b) Transmission x-ray diffraction geometry. (c) Periodic compressions and extensions of the grating pitch characterized by period  $\Lambda = 2\pi/k_x$ . Average pitch is  $d$  and the standard deviation is  $\sigma \approx d\epsilon$ . (d) Primary diffraction peaks are distributed with periodicity  $q_x = 2\pi n/d$ , where  $n$  is an integer, and satellite peaks are adjacent to each primary peak at  $\pm k_x = 2\pi/\Lambda$ .

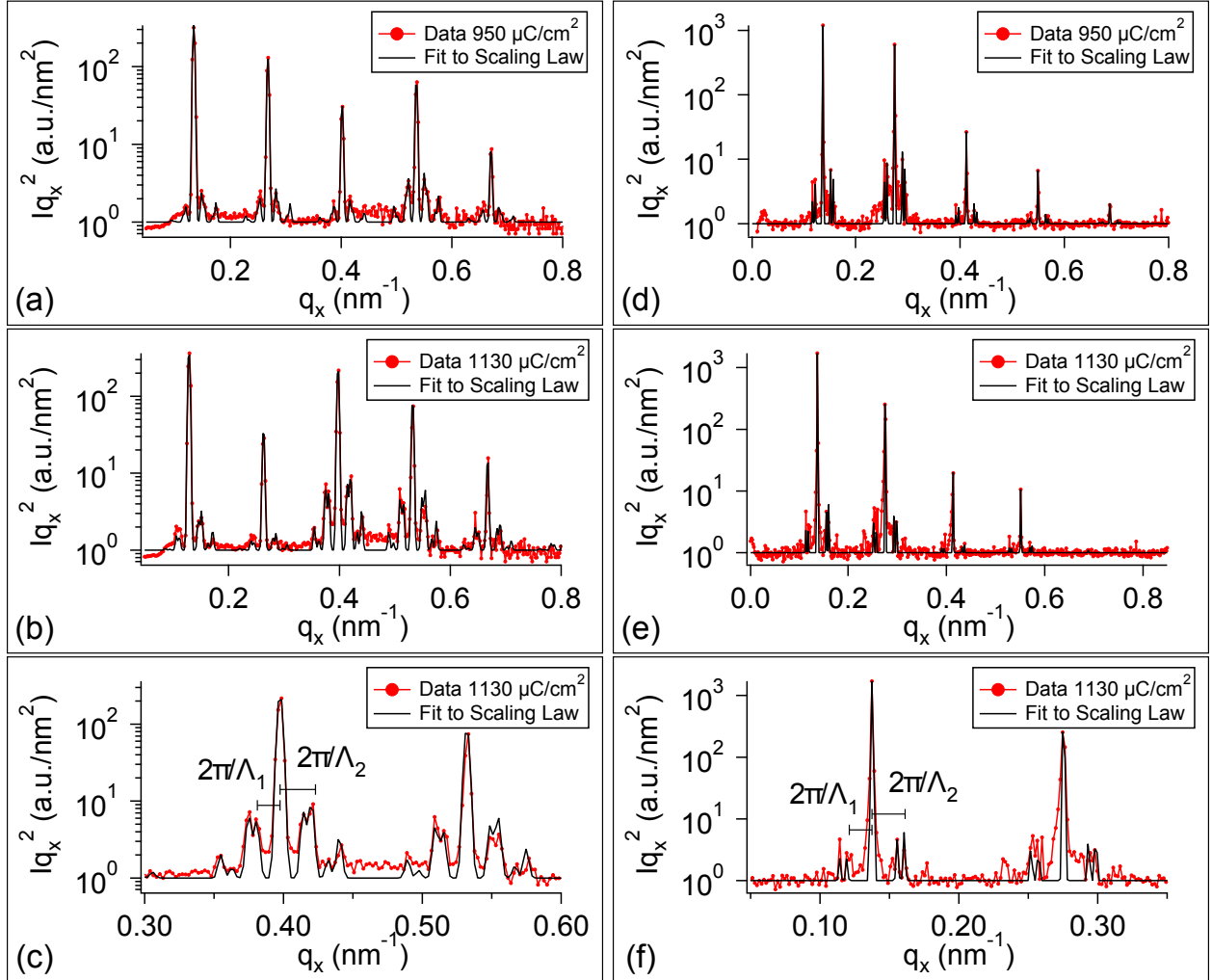


Figure 3: (Full Page) Comparison of XRD data and SEM Fourier transforms. (a,b) Diffraction data from two different ZEP resist gratings and fits to the scaling law in Equation (5). (c) Enlarged region of (b) that shows primary diffraction peaks along with two satellites at  $k_{x,1} = 2\pi/\Lambda_1$  and  $k_{x,2} = 2\pi/\Lambda_2$ . Satellites marked “1” and “2” are associated with noise frequencies  $(62 \pm 2)$  Hz and  $(86 \pm 3)$  Hz, respectively. A third satellite peak associated with ca. 150 Hz noise is visible in these data but was not detected in every sample. (d,e) Fourier transforms of SEM data from two different ZEP resist gratings and fits to the scaling law in Equation (5). (f) Enlarged region of (e) shows primary diffraction peaks along with the two satellites. SEM data are significantly noisier than XRD and do not agree with the  $q^2$ -scaling law.

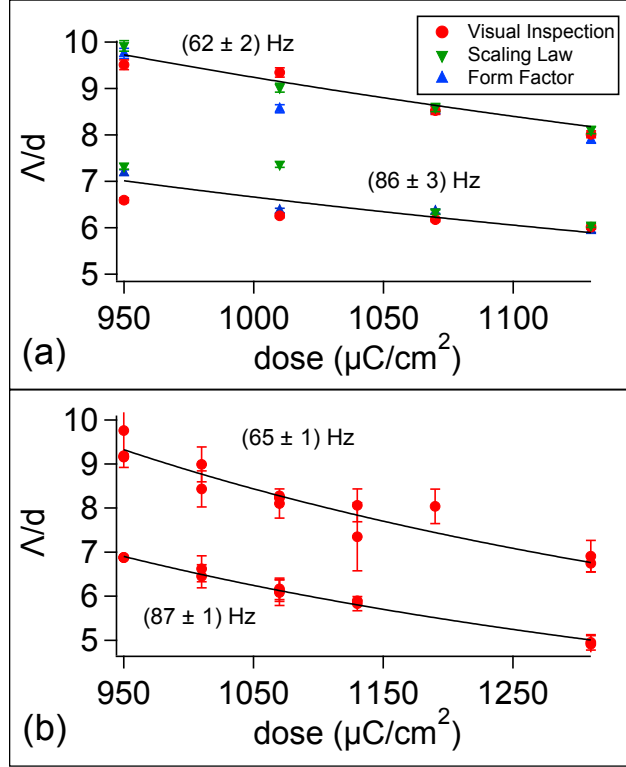


Figure 4: Noise cycles  $\Lambda/d$  for each satellite peak as a function of EBL exposure dose. Solid lines are fits to Equation 7. (a) XRD results. The noise frequencies calculated from visual inspection (red), scaling law (green), and the scaling law with form factor corrections (blue) all closely agree. Error bars represent the uncertainty in determining  $k_x = 2\pi/\Lambda$  from the diffraction data, which is  $0.001 \text{ nm}^{-1}$  by any method. (b) SEM results. Noise frequencies are calculated from visual inspection; other algorithms fail due to SEM image artifacts. Each data point represents the average value of  $k_x$  measured from each image and error bars encompass  $\pm 1$  standard deviation.

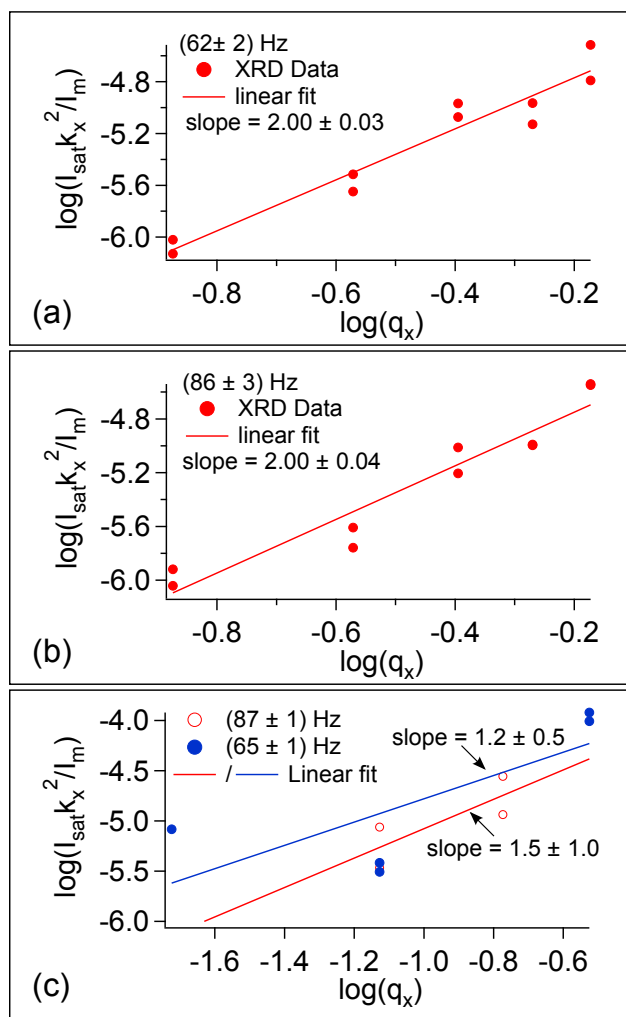


Figure 5: Analysis of ca. 62 Hz and 86 Hz noise in a grating exposed at  $950 \mu\text{C}/\text{cm}^2$ . (a,b) XRD data were analyzed with the “point-and-click” algorithm based on visual inspection. Line is the best fit, and the best-fit slope for both data sets is  $2.0 \pm 0.1$ . This is the slope predicted by the scaling law established with Equation (5). (c) SEM data were analyzed with the algorithm based on visual inspection, but results do not follow the scaling predicted by Equation (5).

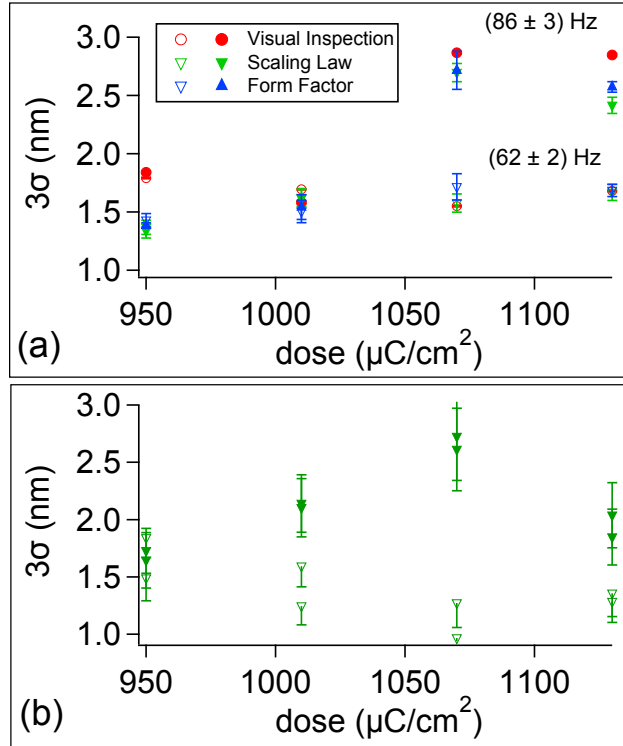


Figure 6: The  $3\sigma$  variation in grating pitch as a function of EBL exposure dose, where  $\sigma$  is the standard deviation. Open and closed symbols correspond with ca. 62 Hz and 86 Hz noise, respectively. (a,b) XRD data analysis. Calculations based on visual inspection (red), scaling law (green), and the scaling law with form factor corrections (blue) all closely agree. Note that 86 Hz noise (mechanical) exhibits greater variation between samples than the 62 Hz noise (electromagnetic). (c) SEM data analysis with the scaling law. Calculated standard deviations are consistent with XRD analysis despite poor agreement between SEM data and the scaling law.